

Microscopic origin of the valence transition in tetragonal EuPd_2Si_2

Young-Joon Song¹, Susanne Schulz², Kristin Kliemt³, Cornelius Krellner³, and Roser Valentí¹

¹*Institut für Theoretische Physik, Goethe-Universität Frankfurt,
Max-von-Laue-Straße 1, 60438 Frankfurt am Main, Germany*

²*Institut für Festkörper- und Materialphysik, Technische Universität Dresden, 01062 Dresden, Germany*

³*Kristall- und Materiallabor, Physikalisches Institut, Goethe-Universität Frankfurt,
Max-von-Laue Straße 1, 60438 Frankfurt am Main, Germany*

(Dated: September 22, 2022)

Under temperature or pressure tuning, tetragonal EuPd_2Si_2 is known to undergo a valence transition from nearly divalent to nearly trivalent Eu accompanied by a volume reduction. Albeit intensive work, its origin is not yet completely understood. Here, we investigate the mechanism of the valence transition under volume compression by density functional theory calculations (DFT). Our analysis suggests that the transition is a consequence of an enhanced c - f hybridization between localized Eu $4f$ states and itinerant conduction states (Eu $5d$, Pd $4d$, and Si $3p$) where the interplay of the electronic bandwidth, crystal field environment, Coulomb repulsion, Hund's coupling and spin-orbit coupling plays a crucial role for the transition to happen. The change in the electronic structure is intimately related to the volume reduction where Eu-Pd(Si) bond lengths shorten. In a next step we compare our DFT results to surface-sensitive photoemission data in which the mixed-valent properties of EuPd_2Si_2 are reflected in a simultaneous observation of divalent and trivalent signals from the Eu $4f$ shell.

I. INTRODUCTION

For decades, $4f$ electron systems have attracted much attention due to the realization of a large variety of interesting phenomena, such as the Kondo effect and emergence of heavy fermion features, quantum criticality, unconventional superconductivity, exotic magnetism, non-trivial topological phases, or valence transitions, to mention a few [1–8]. The latter have been notably investigated in Eu-based systems where Eu can attain two possible valence states; divalent $\text{Eu}^{2+}(4f^7)$ and trivalent $\text{Eu}^{3+}(4f^6)$. In divalent Eu^{2+} , following the Hund's rule in a LS description, seven electrons fill the f states with a total orbital angular momentum $L=0$ and a spin momentum $S=\frac{7}{2}$, giving rise to a total angular momentum $J=\frac{7}{2}$. In trivalent Eu^{3+} , $L=S=3$ and $J=0$.

Upon lowering the temperature a smooth change of the valency from a non-integer value close to a magnetic Eu^{2+} state to a non-integer value close to nonmagnetic Eu^{3+} state has been observed, for instance, in tetragonal EuPd_2Si_2 [9], EuCu_2Si_2 [10, 11], and EuIr_2Si_2 [12, 13]. Alternatively, such valence transitions have been also reported under application of pressure in tetragonal antiferromagnetic (AFM) EuRh_2Si_2 [14], EuNi_2Ge_2 [15], and EuCo_2Ge_2 [16]. While the valence transition is expected to be related to structural and chemical bonding changes between localized $4f$ and the more itinerant s , p and d electrons under temperature or pressure effects, a full understanding of the transition mechanism is still lacking. We focus here on the valence transition in EuPd_2Si_2 .

The valence transition in mixed-valence tetragonal EuPd_2Si_2 was first reported in 1981 in Ref. [9] where a kink in the magnetic susceptibility was observed when lowering the temperature from 200 K to 150 K [9, 17, 18], accompanied by an increase in the Eu average valency [9, 19, 20]. The Curie-Weiss moment of EuPd_2Si_2 at high

temperatures was reported to be $8.04 \mu_B$ [18], which is very close to the theoretically calculated value of $7.94 \mu_B$ for the divalent state ($J = \frac{7}{2}$). It was shown by means of X-ray absorption spectroscopy measurements that at a temperature of about 200 K EuPd_2Si_2 enters into a valence crossover regime with the mean Eu valency changing smoothly from 2.3 to 2.8 between 200 and 100 K [19]. Interestingly, within the valence crossover the lattice parameter $a=4.24 \text{ \AA}$ at room temperature reduces below 50 K to $a=4.16 \text{ \AA}$, whereas c remains unchanged [17, 20, 21] (Fig. 1(a)). The authors of Ref. [22] argued that the valence transition in EuPd_2Si_2 would also occur under application of an external pressure of about 2 GPa, when a reduces to about 4.16 \AA , which is similar to the value of a in the low-temperature regime. Besides, isostructural and isovalent EuPd_2Ge_2 which has a bigger unit cell volume than EuPd_2Si_2 doesn't undergo a valence transition at low temperatures but an AFM transition at $T_N \approx 17 \text{ K}$ [5]. Actually, the tunability of the Eu valence state by applying chemical and finite hydrostatic pressure was reported in single crystals of $\text{EuPd}_2(\text{Si}_{1-x}\text{Ge}_x)_2$ [23]. At $x=0.2$ the long-range AFM order of Eu moments observed below $T_N \approx 47 \text{ K}$ is suppressed by the application of hydrostatic pressure of 0.1 GPa inducing an intermediate valence state in Eu. All these observations point to the important role of the structural changes under temperature or pressure affecting the Eu valency.

In this work we investigate the microscopic origin of the valence transition in EuPd_2Si_2 by a combination of density functional theory (DFT) based calculations and photoemission spectroscopy measurements and show that the transition is a result of an enhanced hybridization between localized Eu $4f$ states and itinerant conduction c states (Eu $5d$, Pd $4d$, and Si $3p$). Moreover, we find that the valence transition is dictated by a delicate interplay of electronic bandwidth, Coulomb repulsion, Hund's

coupling and spin-orbit coupling effects upon volume reduction.

The paper is organized as follows. In Section II we describe the methods used for our study. In Section III we present a comparative analysis of structural details in mixed-valence tetragonal Eu compounds $\text{Eu}TM_2X_2$ where TM denotes the transition metal ion and $X = \text{Si}, \text{Ge}$. In Section IV we present our results on the electronic properties of EuPd_2Si_2 for bulk and slab calculations and compare to experimental photoemission measurements. Finally in Section V we present our conclusions.

II. METHODS

We performed DFT calculations using the full-potential all-electron codes WIEN2k [25], and FPLO [26, 27]. The former code considers a linear augmented plane wave basis to solve the Kohn-Sham equations, while the latter is based on a local-orbital minimum-basis. The exchange-correlation functional was treated within the local (spin) density approximation [L(S)DA] in both WIEN2k and FPLO codes. Crystal bulk structures of EuPd_2Si_2 were fully relaxed in the tetragonal space group $I4/mmm$ within LDA using the *open-core* approximation as implemented in FPLO until forces were smaller than 1 meV/Å. In this approximation the Eu 4*f* states are

removed from the valence basis and enter the bulk description as core orbitals, while fixing the mean 4*f* occupancy n to a given value. The value of n was considered in steps of 0.1 from 6 to 7 in our structural relaxation. Among various n values, we present results for $n=6.7$ ($\text{Eu}^{2.3+}$) as an optimized bulk structure at room temperature, and $n=6.2$ ($\text{Eu}^{2.8+}$) as an optimized structure at low temperature (below 30 K), following the suggested mean valencies from experimental reports in Ref. [9, 19]. The $12 \times 12 \times 12$ k -mesh was adopted for atomic position relaxations, while a dense k -mesh of $21 \times 21 \times 21$ was used for accurate total energy calculations to determine the energetically stable structure. All relaxed lattice parameters obtained at each n value in EuPd_2Si_2 are shown in Fig. 1(c), which agree well with the experimentally observed lattice parameters in dependence of the Eu valence states [17, 20, 21]. Specifically we mention the fully relaxed lattice parameters are $a=4.214$ Å and $c=9.895$ Å at $n=6.7$ ($\text{Eu}^{2.3+}$), and $a=4.128$ Å and $c=9.886$ Å at $n=6.2$ ($\text{Eu}^{2.8+}$). For surface-sensitive electronic structure calculations, we constructed Eu-terminated $1 \times 1 \times 4$ slab structures of EuPd_2Si_2 with a vacuum layer of 15 Å using our optimized bulk structure at room temperature and then relaxed the atomic positions of the four layers close to the surface using the *open-core* approximation with $n=6.7$ for Eu 4*f* within LDA in FPLO.

All electronic and magnetic structures were calculated with WIEN2k including spin-orbit coupling (SOC) and correlation effects (U, J_H) so as to deal with the localized nature of Eu 4*f* orbitals. We fixed $U=6$ eV and the Hund's coupling $J_H=1$ eV for the Eu atom. The k -mesh sampling was $17 \times 17 \times 17$ for the bulk states, and $17 \times 17 \times 1$ for the slab structure. The size of the basis set was determined by the value of $R_{mt}K_{max}=9.0$ with the muffin-tin radius of 2.5(Eu), 2.4(Pd), 1.95(Si), and 2.25(Ge) in atomic units.

In order to describe divalent states (Eu^{2+}) in DFT, the inclusion of spin degrees of freedom in spin-polarized calculations was taken into account for simulation purposes, even though EuPd_2Si_2 at room temperature doesn't magnetically order. We assumed ferromagnetic (FM) spin order with an easy axis parallel to the z -axis. In addition, for the comparison of the electronic structures between EuPd_2Si_2 and EuPd_2Ge_2 , an A-type AFM spin order where the Eu magnetic ions are ferromagnetically aligned within the ab plane and antiferromagnetically aligned between consecutive planes was set. The corresponding magnetic space group is $P4_1/mnc$ (No.128.410). For these calculations, we also fully relaxed the EuPd_2Ge_2 crystal bulk structures as we did in EuPd_2Si_2 . The fully relaxed lattice parameters in EuPd_2Ge_2 at $n=7$ are $a=4.344$ Å and $c=10.217$ Å which are also in good agreement with experiment ($a_{exp}=4.3764$ Å and $c_{exp}=10.072$ Å) [5].

Single crystals of EuPd_2Si_2 were grown using the Czochralski method according to the procedure described in [21]. Angular-resolved photoemission measurements (ARPES) on the (001) surface were performed at the 1³

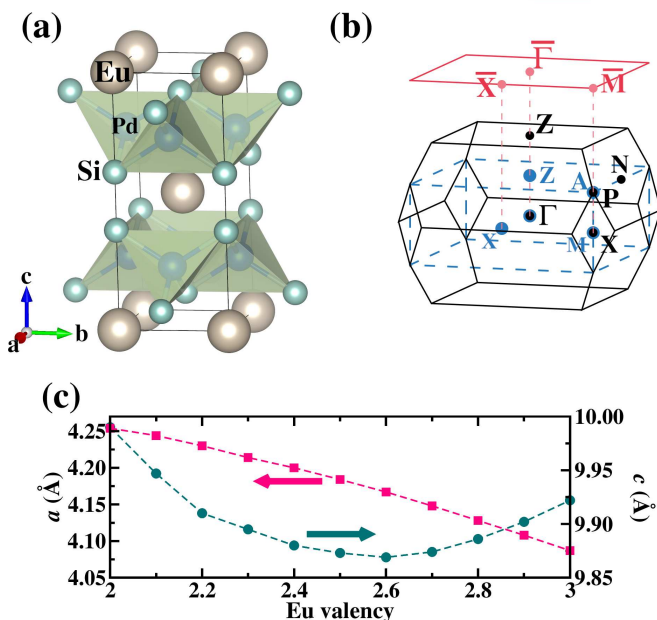


FIG. 1. (a) Crystal structure of tetragonal EuPd_2Si_2 , produced by VESTA [24]. (b) First Brillouin zone of the tetragonal $I4/mmm$ (black, solid) and $P4/mmm$ (blue, dashed) structure with special k points for the band structure. The (001) surface was projected in the slab calculations, which is drawn by a pink rectangle. (c) Fully relaxed lattice parameters of EuPd_2Si_2 at each Eu valency obtained using the *open-core* approximation within LDA.

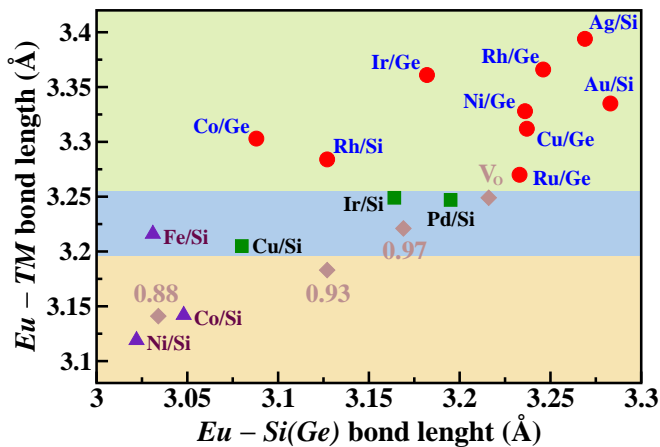


FIG. 2. Classification of tetragonal Eu compounds EuTM_2X_2 according to their experimentally reported Eu-TM and Eu-X bond lengths, where $\text{TM} = \text{Fe}, \text{Co}, \text{Ni}, \text{Cu}, \text{Ru}, \text{Rh}, \text{Pd}, \text{Ag}, \text{Ir}, \text{Au}$, and $\text{X} = \text{Si}, \text{Ge}$. Data were obtained from, respectively, $\text{TM/X} = \text{Ni/Si}$ [30], Co/Si [31], Fe/Si [32], Cu/Si [33], Co/Ge [34], Ir/Si [13], Rh/Si [35], Pd/Si [36], Ir/Ge [37, 38], Ru/Ge [37, 39], Cu/Ge [40, 41], Ni/Ge [32, 34], Rh/Ge [39, 42], Au/Si [43, 44], Ag/Si [43, 45]. Systems with divalent $\text{Eu}^{2+\delta}$ states at low temperatures are shown by red circles, whereas purple triangles denote trivalent $\text{Eu}^{3-\delta}$ compounds. Green squares indicate compounds which undergo a valence transition by varying temperature. Brown rhombuses indicate bond lengths of relaxed EuPd_2Si_2 at a given volume with respect to the relaxed one (V_0) calculated for $n=6.7$ (see Methods section). Below $0.93V_0$, bond lengths become similar to those of trivalent Eu compounds.

ARPES instrument at BESSY II [28]. To prepare a clean surface the samples were cleaved in-situ under ultra-high vacuum conditions at a temperature of 41 K.

III. STRUCTURAL DETAILS

EuPd_2Si_2 crystallizes in a tetragonal body-centered ThCr_2Si_2 -type [29] structure with space group $I4/mmm$ (No.139) [17]. It consists of layers of edge-sharing PdSi_4 tetrahedra intercalated between Eu planes, as shown in Fig. 1(a). Eu, Pd and Si are at Wyckoff positions $2a$, $4d$, and $4e$ ($z_{\text{rel}}=0.3779$ for $\text{Eu}^{2.3+}$ and 0.3818 for $\text{Eu}^{2.8+}$) respectively). Similar to Si, Ge in EuPd_2Ge_2 also sits on the $4e$ site with $z_{\text{rel}}=0.3715$ for Eu^{2+} .

The valence transition in EuPd_2Si_2 is accompanied by a volume contraction where the lattice parameter a shrinks from $a=4.24$ Å at room temperature to $a=4.16$ Å below 50 K. In order to study the relation between volume contraction (and corresponding atomic bond-lengths shortening) with the valence transition, we collected in Fig. 2 crystal information of ThCr_2Si_2 -type tetragonal Eu-based compounds EuTM_2X_2 whose valence states are confirmed experimentally. Fig. 2 illustrates two kinds of bond lengths between Eu and the transition metal (TM) ion, and between Eu and the

carbon-group (X) ion, respectively. Red circles indicate tetragonal Eu compounds that show magnetic ground states (e.g. with divalent $\text{Eu}^{2+\delta}$), whereas purple triangles are nonmagnetic ($\text{Eu}^{3-\delta}$) compounds. Systems undergoing a valence transition when temperature decreases are marked by green squares. The following compounds undergo a pressure-induced valence transition at pressures of about 1 GPa for EuRh_2Si_2 [14], 2 GPa for EuNi_2Ge_2 [15], and 3 GPa for EuCo_2Ge_2 [16]. Furthermore, recent surface-sensitive photoemission experiments on tetragonal EuIr_2Si_2 , marked by a green square in Fig. 2, reveal divalent Eu^{2+} states in the surface region with two-dimensional ferromagnetic order at low temperatures, while in the bulk Eu is almost trivalent and has a nonmagnetic ground state. [46, 47].

Interestingly, EuCu_2Si_2 , denoted by a green square in Fig. 2, has been reported to show a valence transition by lowering temperature [10, 11], however, while Ref. [48] reported the appearance of Eu antiferromagnetism at 10 K in single crystals, the authors of Ref. [49] suggested that the appearance of volume contractions and corresponding change of Eu valence states at low temperatures originate from the crystallization method and crystal defects. These authors confirmed the presence of trivalent states on a single crystal EuCu_2Si_2 at low temperatures. Actually, the single crystal from Ref. [48] has a larger volume by about 3 % compared to the samples showing trivalent states [49]. Recently, it was found experimentally that bond lengths and valence transition temperature in EuPd_2Si_2 can also change depending on the amount of disorder in the Pd-Si layer [21].

Summarizing the above observations, the Eu valence state in these tetragonal Eu-based compounds is intimately related to the value of Eu-TM and Eu-X bond lengths in the systems. In what follows we concentrate on EuPd_2Si_2 and analyze via *ab initio* DFT the Eu valence transition under volume reduction.

IV. ELECTRONIC STRUCTURE

A. Calculations for bulk EuPd_2Si_2

We start by examining the description of Eu $4f$ states in the context of competing Coulomb interaction, crystal field environment and spin-orbit coupling at ambient pressure. As it is known from atomic physics [50], the description of the electronic structure of an atom depends on the hierarchy of the involved interactions. In the case that the Coulomb interaction between the electrons is stronger than the spin-orbit interactions in each of them, then the total angular momentum $L = \sum_i l_i$ and total spin $S = \sum_i s_i$ of the electron system, where l_i and s_i are, respectively, the angular momentum and spin of each individual electron, couple to a total J . This situation corresponds to the LS description. If, however, the individual electron coupling via the spin-orbit interaction is stronger than the Coulomb interaction between elec-

trons U_{ee} , then the individual total momenta $j_i = l_i + s_i$, couple to a total $J = \sum_i j_i$ which corresponds to a jj description. Usually the former description is valid for light atoms, while the latter is more appropriate for heavy atoms. In $4f$ systems U_{ee} is usually larger than the SOC constant ξ_{SOC} and the LS coupling scheme may be more appropriate [51]. Actually, in a LS description Eu^{2+} ($4f^7$) has $S = 7/2$, $L = 0$ and a total $J = 7/2$. Alternatively, in the jj description j_i with $i = 1, 2, \dots, 7$ can take values $5/2$ and $7/2$ and the total J in the ground state is then $J = 7/2$ as well. Analogously Eu^{3+} ($4f^6$) in a LS description has $S = L = 3$ and $J = 0$. Considering the jj description, j_i , $i = 1, 2, \dots, 6$ it results in $J = 0$. The differences between the two schemes is perceived when investigating the magnetic moments [51] $M = g_J \mu_B J$ where the Landé factor g_J corresponds to the electron gyromagnetic factor $g_J = 2$ in the LS scheme, while in the jj coupling $g_J = 8/7$ for Eu^{2+} . These nuances in the description are important when comparing the calculated magnetic properties to experiment.

Now we analyze the limiting case of the relaxed structure obtained for $n = 6.7$ (see Methods section) corresponding to EuPd_2Si_2 at ambient pressure and ambient temperature [19]. Fig. 3(a) shows the LSDA+SOC+ U calculated electronic structure and corresponding orbital projected densities of states (DOSs) for EuPd_2Si_2 where we assumed a FM configuration for Eu. Due to the half-filled shell ($4f^7$), the fully occupied $4f$ bands in the majority spin channel (colored pink in Fig. 3(a)) are centered around -1.0 eV below the Fermi level with a bandwidth of about 1 eV. Note that the energy of the calculated $4f$ states corresponds to the energy position of the Eu^{2+} final-state multiplet seen in photoemission, Fig. 5(b).

Furthermore, in this energy range, itinerant conduction states of Pd $4d$, Si $3p$, and Eu $5d$ are present, which hybridize with the half-filled Eu $4f$ bands. Specifically, there is a hole pocket with dominant Eu $5d$ character at the Γ point, as well as electron pockets with dominant Pd $4d$ and Si $3p$ characters at around the X and P points. The calculated total spin moment (M_S) is $6.95 \mu_B/\text{Eu}$ with a negligible angular moment of $-0.024 \mu_B/\text{Eu}$, which is in good agreement with the values of $S = \frac{7}{2}$ and $L = 0$ expected from the Hund's rule in the divalent Eu^{2+} state in the LS scheme. Specifically, the occupation numbers of each orbital are 6.716 for Eu $4f$, 8.016 for Pd $4d$, 0.815 for Si $3p$, and 0.331 for Eu $5d$ orbitals. In contrast to EuPd_2Si_2 , EuPd_2Ge_2 doesn't undergo a valence transition at low temperatures but an AFM transition at $T_N = 17$ K [5]. This is directly related to the fact that Eu-Pd / Eu-Ge bond lengths in EuPd_2Ge_2 are longer than Eu-Pd / Eu-Si bond lengths in EuPd_2Si_2 and, following Fig. 2, Eu^{2+} states are expected. Our relaxed bond lengths of Eu-Pd / Eu-Ge in EuPd_2Ge_2 differ by 3.2 / 3.9% from those of Eu-Pd / Eu-Si in EuPd_2Si_2 . Figure 3(d) illustrates band structures and Eu $4f$ orbital projected DOS of A-AFM EuPd_2Si_2 (black) and EuPd_2Ge_2 (cyan) within LSDA+SOC+ U . Due to the longer bond

lengths, $4f$ states in EuPd_2Ge_2 near the Fermi level are less dispersive and have a smaller bandwidth than those of EuPd_2Si_2 .

We consider now the relaxed EuPd_2Si_2 structure at $n=6.2$ (see Methods section). To obtain the electronic structure we performed calculations within LSDA+SOC+ U ($U = 6$ eV, $J_H = 1$ eV), with zero initial magnetization for the Eu atom. Both combined effects, SOC and correlation (U) shift down the occupied sixfold $|j = \frac{5}{2}\rangle$ states to about 6.4 eV below the Fermi level and show almost no dispersion, whereas the empty eightfold $|j = \frac{7}{2}\rangle$ states are located around 1.6 eV above the Fermi level, not shown here. With the choice of U and J_H values above, the energy position of the occupied $|j = \frac{5}{2}\rangle$ states coincides with the position of the trivalent Eu states in photoemission measurements (compare to Fig. 5(b)). Note however that in Fig. 5(b), due to the multiplet nature of trivalent Eu, two separated main peaks are observed at about 7 eV below the Fermi level. This feature is not captured in the DFT calculations, due to the limitations of the method to describe manybody multiplet states.

B. Role of volume reduction on the hybridization

We analyze now the effect of volume reduction on the valence transition from divalent Eu to trivalent Eu in EuPd_2Si_2 . As mentioned above, this system undergoes a valence transition by lowering temperature or by increasing pressure [9, 22]. Both effects reduce the volume in EuPd_2Si_2 , implying a shortening of the Eu-Pd and Eu-Si bond lengths.

To investigate how the volume reduction affects the electronic structure and the valence state of EuPd_2Si_2 , we obtained a few bulk EuPd_2Si_2 structures with a smaller volume than our fully relaxed one (V_o) at $n = 6.7$ by relaxing them using the *open-core* approximation as implemented in FPLO within LDA. Our fully relaxed lattice parameters at $n=6.7$ ($\text{Eu}^{2.3+}$), which correspond to the room temperature bulk structure at ambient pressure are $a=4.214$ and $c=9.895$ Å as given in the Methods section with bond lengths of Eu-Pd=3.25 Å and Eu-Si=3.22 Å. Note that the Eu-Si bond length is in good agreement with our value determined in [21]. These bond lengths are marked by a brown rhombus with V_o in Fig. 2. These values are slightly larger than the reported ones in the literature [36]. Also plotted in Fig. 2 are the results for relaxed structures at a volume of $0.97V_o$, $0.93V_o$, and $0.88V_o$. We note that the lattice parameter a for the crystal structure relaxed at $0.97V_o$ is similar to the experimentally reported one at a temperature below 30 K and 0 GPa when the system has undergone the valence transition and has experienced a volume contraction. The values of bond lengths are in the same range as those for compounds that undergo a valence transition (marked by green squares in Fig. 2).

Fig. 3(a) and (b) show the fat band electronic struc-

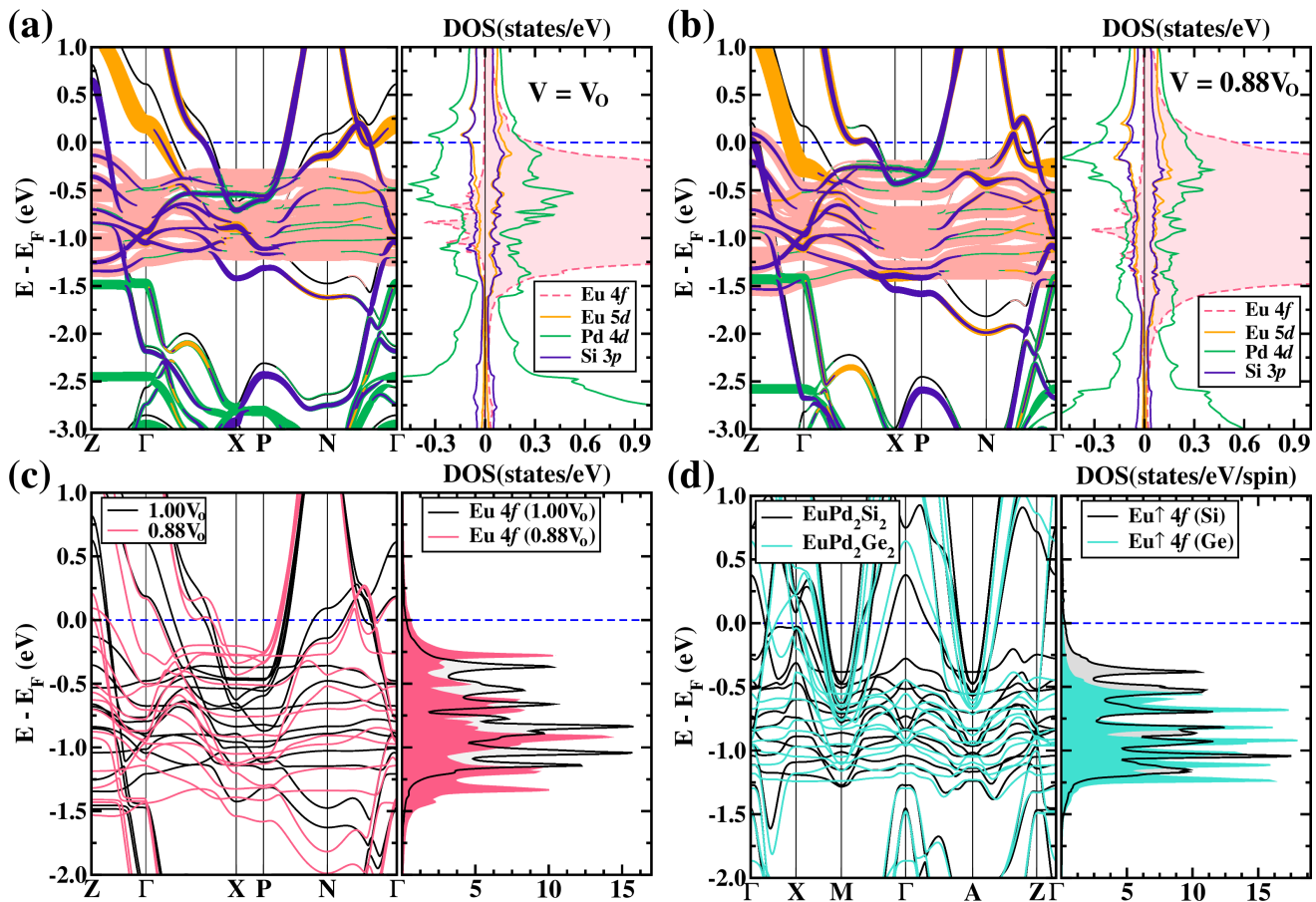


FIG. 3. Fat band electronic structures and orbital projected DOSs obtained from LSDA+SOC+ U for EuPd₂Si₂ (a-c) and EuPd₂Ge₂ (d). (a) FM band structures for EuPd₂Si₂ at V_o ($n = 6.7$ relaxed structure, see Methods section) and (b) at a volume of $0.88V_o$. At V_o in (a), the occupied spin-up Eu 4*f* bands in the FM results are located just below the Fermi level. The energy position of the Eu 4*f* states is in good agreement with photoemission results, as shown in Fig. 5(b). At $0.88V_o$, the c - f hybridization is enhanced leading to a larger bandwidth of 4*f* bands in (b). The weight of Eu 4*f* band characters (a-b) was scaled by a factor of 0.25 for clarity. (c) Overlapped band structures and Eu 4*f* orbital projected DOSs within LSDA+SOC+ U for EuPd₂Si₂ at V_o (black color) and at $0.88V_o$ (light red color). The volume reduction in EuPd₂Si₂ with shorter bond lengths induces an enhanced c - f hybridization leading to more dispersive bands and a larger bandwidth of Eu 4*f*. (d) Overlapped band structures and orbital projected DOSs for EuPd₂Si₂ (black color) and EuPd₂Ge₂ (cyan color) at V_o both calculated in the A-AFM state. Longer bond lengths in EuPd₂Ge₂ lead to more localized Eu 4*f* states.

ture and orbital projected DOSs of FM EuPd₂Si₂ in LSDA+SOC+ U at a volume of V_o and $0.88V_o$, respectively. The majority 4*f* bands are located just below the Fermi level. Compared to the V_o results, at $0.88V_o$ the 4*f* bandwidth is somewhat larger and more dispersive with an enhanced c - f hybridization. This can be better observed in Fig. 3(c) where we superimposed both electronic structure contributions. Specifically, a reduction of volume leads to a decrease of the occupation number of Eu 4*f* states, whereas the occupation number in the other orbitals goes up, as shown in Fig. 4 where we display the occupation of Eu 4*f*, Pd 4*d*, Si 3*p*, and Eu 5*d* states as a function of volume. This is directly related to a shortening of the Eu-*TM* and Eu-*X* bond lengths, (see brown rhombuses in Fig. 2) and an enhanced hybridization between Eu 4*f* and the itinerant conduction states (Eu 5*d*, Pd 4*d*, and Si 3*p*). Further, under volume

reduction the total spin moment decreases, whereas the orbital moment increases in magnitude. (See Fig. 4(b)) At $0.88V_o$, the orbital moment of Eu becomes $-0.152 \mu_B/\text{Eu}$ which is a consequence of a slight decrease of the occupation of a mostly $|3, 3\rangle$ state, whereas the occupation of the other states remains nearly unchanged. Furthermore, the orbital moment increases to $-0.228 \mu_B/\text{Eu}$ at $0.82V_o$. This behavior shows a tendency to follow the Hund's rules for Eu³⁺ which is $L=S=3$ and $J = |S - L| = 0$.

We conclude this section by the observation that an LS scheme is more suitable to describe the electronic structure of EuPd₂Si₂ with Eu in the nearly divalent state, while in the case of Eu in a nearly trivalent state corresponding to the reduced volume case, the jj coupling scheme seems more appropriate, as discussed in Ref. [51]. The reason for that is the relative changes in the ra-

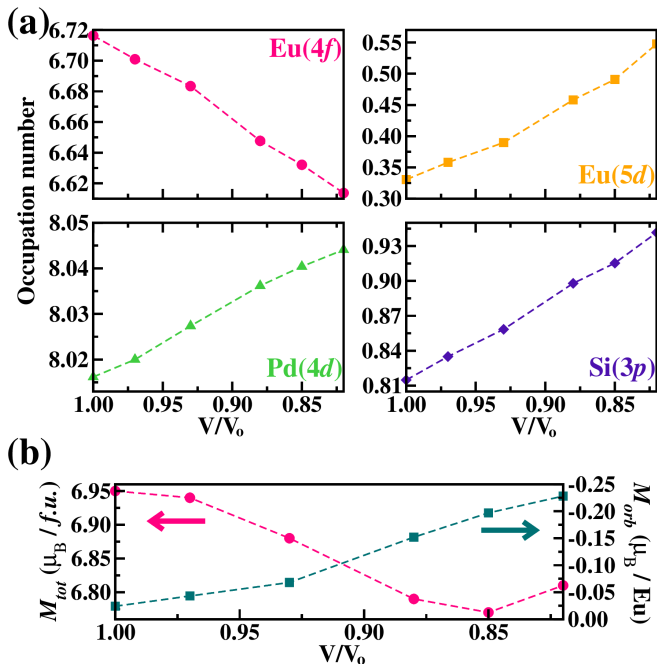


FIG. 4. (a) Occupation number of each orbital as a function of volume reduction of EuPd_2Si_2 within LSDA+SOC+ U where V_o corresponds to the structure relaxed with $n = 6.7$ (see Methods section). When the volume is reduced, the number of occupied Eu $4f$ states decreases, whereas there is an increase in the other states. (b) Corresponding total spin moment and orbital moment of Eu as a function of volume compression. A decrease of volume results in a decrease of the total spin moment, whereas the orbital moment of Eu increases in magnitude.

tio ξ_{SOC}/U_{ee} [51] where ξ_{SOC} is the spin-orbit coupling strength and U_{ee} the Coulomb interaction. This ratio increases at reduced volumes, as happens while lowering temperature, due to an increased $c-f$ hybridization.

C. Photoemission from the $4f$ shell

Recently, some of us [46] reported two-dimensional ferromagnetism at a temperature below 48 K in a single Eu layer located below the iridium-silicide surface of tetragonal EuIr_2Si_2 , which shows a temperature-driven valence crossover (marked by a green square in Fig. 2), whereas bulk regions display no magnetism due to the presence of Eu^{3+} . In a later experiment, surface ferromagnetism was observed at the Eu-terminated surface of EuIr_2Si_2 as well [47]. Fig. 5(b) shows an ARPES spectrum acquired from the (001) surface of a freshly cleaved EuPd_2Si_2 single crystal at a temperature of 41 K. Although the compound was first synthesized decades ago, only recently large single crystals are available [21], enabling ARPES measurements. On the right-hand side the angle-integrated spectrum is plotted. To maximally enhance the emission from the $4f$ shell

over contributions from the valence band we used a photon energy of 145 eV which corresponds to the maximum of the $4d \rightarrow 4f$ Fano-Beutler resonance of Eu^{3+} . Note that at the given photon energy the $4f$ emission of Eu^{2+} is resonantly enhanced too. In the spectrum, three dominating non-dispersive $4f$ features are present: (1) The straight line at the Fermi level represents the $4f^7 \rightarrow 4f^6$ final-state multiplet of Eu^{2+} in bulk-like layers; (2) The most intense line at a slightly higher binding energy of about 1 eV is the surface-core-level shifted $4f$ emission of Eu^{2+} at the surface; (3) The broad structure consisting of several lines between 6 and 10 eV forms the $4f^6 \rightarrow 4f^5$ final-state multiplet of Eu^{3+} in bulk-like layers. The simultaneous observation of both the Eu^{2+} and Eu^{3+} final-state multiplets reflects the mixed-valent properties of Eu in this compound.

D. Slab calculations

To understand the observations from surface-sensitive ARPES measurements presented in the previous section, we constructed a $1 \times 1 \times 4$ Eu-terminated slab geometry as described in the Methods section. Due to the symmetric geometry, where the space group of this slab structure is $P4/mmm$, there are five inequivalent Eu atoms in the unit cell. Numbering these Eu atoms in relation to proximity to the surface, they are represented by Eu1 through Eu5 with Eu1 at the surface and Eu5 situated furthest from the surface *i.e.* located at the center of the unit cell. For the calculation of the electronic structure, we considered FM configurations of these Eu atoms as in our bulk calculations. Figure 5(a) illustrates the (001)-projected band structure and Eu $4f$ orbital resolved DOS of the slab structure described above for the FM spin configuration in LSDA+SOC+ U . All nearly divalent Eu $4f$ states appear at around 1 eV below the Fermi level. Interestingly, $4f$ states of Eu2, Eu3, Eu4, Eu5 states belonging to the bulk are much closer to the Fermi level than those of Eu1 at the surface. In this case, the on-site energy of the $4f$ states was calculated as -1.31 eV for Eu1 and about -0.8 eV for the rest of Eu. This result is in good agreement with our PES results, shown in Fig. 5(b), where a peak from Eu^{2+} (surface) is farther from the Fermi level than that from bulk. We would like to stress that these separated $4f$ states are a result of the slab geometry and the fact that the bond lengths of Eu-Pd(Eu-Si) are different between Eu1 and Eu2, Eu3, Eu4, Eu5

V. CONCLUSIONS

In this work we have investigated the mechanism of the valence transition in the testbed system EuPd_2Si_2 which is known to undergo a valence transition from nearly divalent Eu to nearly trivalent Eu upon lowering the tem-

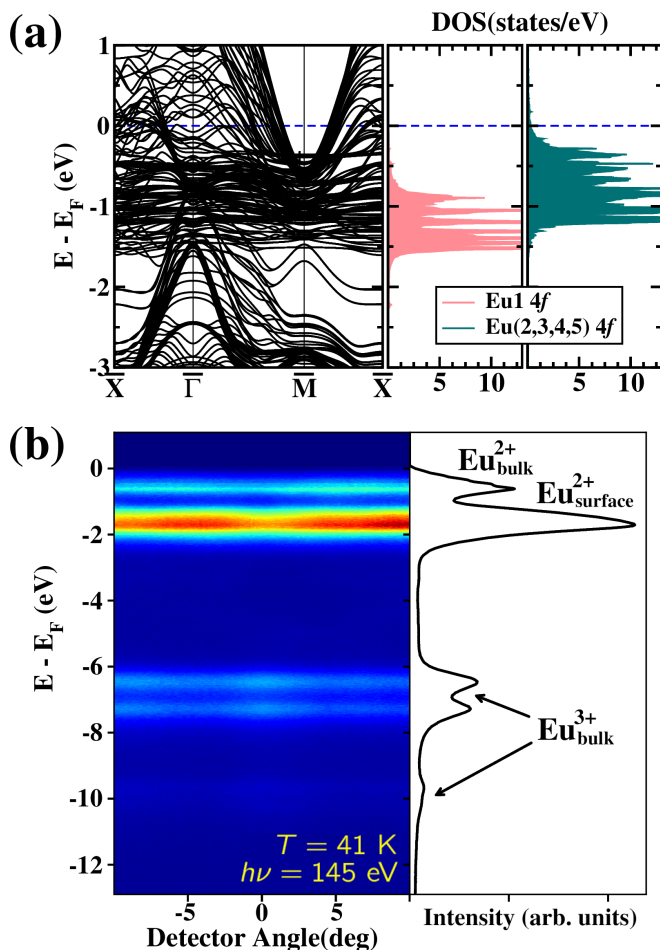


FIG. 5. (a) LSDA+SOC+ U electronic band structure and $4f$ orbital projected DOS of the Eu-terminated $1 \times 1 \times 4$ slab structure with a spin configuration where all Eu atoms were set to be of FM order. (b) ARPES spectrum acquired with $h\nu = 145$ eV at a temperature of 41 K from the (001) surface of EuPd_2Si_2 for a mixture of Si- and Eu-terminated areas, that shows the Eu $4f$ emission. On the right the angle-integrated spectrum is given.

perature. By making use of the observation that the valence transition is accompanied by a volume contraction, we studied the valence transition by a combination of (i) density functional theory calculations where we considered volume contracted structures, and (ii) photoemission measurements taken at $T = 41$ K with $h\nu = 145$ eV. Our results show that a decrease of Eu-Pd(Si) bond lengths resulting from a volume contraction induces an enhanced $c-f$ hybridization between localized Eu $4f$ states and itinerant conduction states (Eu $5d$, Pd $4d$, and Si $3p$). As the bond lengths get shorter the occupation number of the Eu $4f$ states decreases whereas that of the conduction states increases. We conclude that the redistribution of electronic weight and Eu valence crossover is dictated by a delicate interplay of the electronic bandwidth, crystal field environment, Coulomb repulsion, Hund's coupling and spin-orbit coupling effects.

Further, our DFT EuPd_2Si_2 bulk and Eu-terminated slab results are in good agreement with our surface sensitive photoemission experiments reproducing the presence of divalent Eu states near the Fermi level coming from surface/bulk Eu and of trivalent Eu states at high binding energies developing from bulk Eu.

VI. ACKNOWLEDGMENTS

We thank Daniel Khomskii, Michael Lang, Igor Mazin and Bernd Wolf for useful discussions. Y.-J. S., K.K., C.K. and R.V. acknowledge support by the Deutsche Forschungsgemeinschaft (DFG, German Research Foundation) for funding through TRR 288 – 422213477 (projects A03, A05). S.S. acknowledges DFG support through Grant No. KR3831/5-1. We thank the Helmholtz-Zentrum Berlin für Materialien und Energie for the allocation of synchrotron radiation beamtime.

- [1] S. Wirth and F. Steglich, Exploring heavy fermions from macroscopic to microscopic length scales, *Nat. Rev. Mater.* **1**, 16051 (2016).
- [2] J. G. Rau and M. J. Gingras, Frustrated quantum rare-earth pyrochlores, *Annu. Rev. Condens. Matter. Phys.* **10**, 357 (2019).
- [3] C. Pfleiderer, Superconducting phases of f -electron compounds, *Rev. Mod. Phys.* **81**, 1551 (2009).
- [4] G. R. Stewart, Non-Fermi-liquid behavior in d - and f -electron metals, *Rev. Mod. Phys.* **73**, 797 (2001).
- [5] Y. Ōnuki, M. Hedo, and F. Honda, Unique electronic states of Eu-based compounds, *J. Phys. Soc. Jpn.* **89**, 102001 (2020).
- [6] Y. Ōnuki, A. Nakamura, F. Honda, D. Aoki, T. Tekeuchi, M. Nakashima, Y. Amako, H. Harima, K. Matsubayashi, Y. Uwatoko, S. Kayama, T. Kagayama, K. Shimizu, S. Esakki Muthu, D. Braithwaite, B. Salce, H. Shiba, T. Yara, Y. Ashitomi, H. Akamine, K. Tomori, M. Hedo, and T. Nakama, Divalent, trivalent, and heavy fermion states in Eu compounds, *Philos. Mag.* **97**, 3399 (2017).
- [7] Y. Xu, L. Elcoro, Z.-D. Song, B. J. Wieder, M. G. Vergniory, N. Regnault, Y. Chen, C. Felser, and B. A. Bernevig, High-throughput calculations of magnetic topological materials, *Nature* **586**, 702 (2020).
- [8] M. C. Rahn, J.-R. Soh, S. Francoual, L. S. I. Veiga, J. Stremper, J. Mardegan, D. Y. Yan, Y. F. Guo, Y. G. Shi, and A. T. Boothroyd, Coupling of magnetic order and charge transport in the candidate Dirac semimetal EuCd_2As_2 , *Phys. Rev. B* **97**, 214422 (2018).
- [9] E. V. Sampathkumaran, L. C. Gupta, R. Vijayaraghavan, K. V. Gopalakrishnan, R. G. Pillay, and H. G. Devare, A new and unique Eu-based mixed valence system: EuPd_2Si_2 , *J. Phys. C: Solid State Phys.* **14**, L237 (1981).
- [10] E. R. Bauminger, D. Froindlich, I. Nowik, S. Ofer, I. Felner, and I. Mayer, Charge Fluctuations in Europium in Metallic EuCu_2Si_2 , *Phys. Rev. Lett.* **30**, 1053 (1973).
- [11] S. Patil, R. Nagarajan, C. Godart, J. P. Kappler, L. C. Gupta, B. D. Padalia, and R. Vijayaraghavan, Valence fluctuation in the dilute Eu systems $\text{Eu:RPd}_2\text{Si}_2$, $\text{Eu:RCu}_2\text{Si}_2$, and Eu:RNiSi_2 ($R=\text{La, Y, and Yb}$), *Phys. Rev. B* **47**, 8794 (1993).
- [12] B. Chevalier, J. M. D. Coey, B. Lloret, and J. Etourneau, EuIr_2Si_2 : a new intermediate valence compound, *J. Phys. C: Solid State Phys.* **19**, 4521 (1986).
- [13] S. Seiro, Y. Prots, K. Kummer, H. Rosner, R. Cardoso Gil, and C. Geibel, Charge, lattice and magnetism across the valence crossover in EuIr_2Si_2 single crystals, *J. Phys.: Condens. Matter* **31**, 305602 (2019).
- [14] A. Mitsuda, S. Hamano, N. Araoka, H. Yayama, and H. Wada, Pressure-Induced Valence Transition in Antiferromagnet EuRh_2Si_2 , *J. Phys. Soc. Jpn.* **81**, 023709 (2012).
- [15] A. Nakamura, T. Nakama, K. Uchima, N. Arakaki, C. Zukeran, S. Komesu, M. Takeda, Y. Takaesu, D. Nakamura, M. Hedo, K. Yagasaki, and Y. Uwatoko, Effect of pressure on thermopower of EuNi_2Ge_2 , *J. Phys.: Conf. Ser.* **400**, 032106 (2012).
- [16] G. Dionicio, H. Wilhelm, Z. Hossain, and C. Geibel, Temperature- and pressure-induced valence transition in EuCo_2Ge_2 , *Physica B* **378-380**, 724 (2006).
- [17] A. Palenzona, S. Cirafici, and F. Canepa, High Temperature Behaviour of Unstable EuPd_2Si_2 and Reference MPd_2Si_2 Compounds ($M \equiv$ All Rare Earths and Alkaline Earths), *J. Less-Common Met.* **135**, 185 (1987).
- [18] A. Mitsuda, H. Wada, M. Shiga, H. Aruga Katori, and T. Goto, Field-induced valence transition of $\text{Eu}(\text{Pd}_{1-x}\text{Pt}_x)_2\text{Si}_2$, *Phys. Rev. B* **55**, 12474 (1997).
- [19] K. Mimura, Y. Taguchi, S. Fukuda, A. Mitsuda, J. Sakurai, K. Ichikawa, and O. Aita, Bulk-sensitive high-resolution photoemission study of a temperature-induced valence transition system EuPd_2Si_2 , *J. Electron Spectrosc. Relat. Phenom.* **137-140**, 529 (2004).
- [20] A. Mitsuda, H. Wada, M. Shiga, and T. Tanaka, The Eu valence state and valence transition in $\text{Eu}(\text{Pd}_{1-x}\text{Pt}_x)_2\text{Si}_2$, *J. Phys.: Condens. Matter* **12**, 5287 (2000).
- [21] K. Kliemt, M. Peters, I. Reiser, M. Ocker, F. Walther, D.-M. Tran, E. Cho, M. Merz, A. A. Haghighirad, D. C. Hezel, F. Ritter, and C. Krellner, Influence of the Pd-Si Ratio on the Valence Transition in EuPd_2Si_2 Single Crystals, *Cryst. Growth Des.* **22**, 5399 (2022).
- [22] D. M. Adams, A. E. Heath, H. Jhans, A. Norman, and S. Leonard, The effect of high pressure upon the valence transition in EuPd_2Si_2 , *J. Phys.: Condens. Matter* **3**, 5465 (1991).
- [23] B. Wolf, F. Spathelf, J. Zimmermann, T. Lundbeck, M. Peters, K. Kliemt, C. Krellner, and M. Lang, From magnetic order to valence-change crossover in $\text{EuPd}_2(\text{Si}_{1-x}\text{Ge}_x)_2$ using He-gas pressure, *SciPost*, 00023v1 (2022).
- [24] K. Momma and F. Izumi, *VESTA 3* for three-dimensional visualization of crystal, volumetric and morphology data, *J. Appl. Crystallogr.* **44**, 1272 (2011).
- [25] P. Blaha, K. Schwarz, F. Tran, R. Laskowski, G. K. H. Madsen, and L. D. Marks, WIEN2k: An APW+lo program for calculating the properties of solids, *J. Chem. Phys.* **152**, 074101 (2020).
- [26] K. Koepnik and H. Eschrig, Full-potential nonorthogonal local-orbital minimum-basis band-structure scheme, *Phys. Rev. B* **59**, 1743 (1999).
- [27] I. Opahle, K. Koepnik, and H. Eschrig, Full-potential band-structure calculation of iron pyrite, *Phys. Rev. B* **60**, 14035 (1999).
- [28] S. V. Borisenko, "One-cubed" ARPES User Facility at BESSY II, *Synchrotron Radiation News* **25**, 6 (2012).
- [29] Z. Ban and M. Sikirica, The crystal structure of ternary silicides ThM_2Si_2 ($M = \text{Cr, Mn, Fe, Co, Ni}$ and Cu), *Acta Cryst.* **18**, 594 (1965).
- [30] G. Wortmann, I. Nowik, B. Perscheid, G. Kaindl, and I. Felner, Critical evaluation of Eu valences from L_{III} -edge X-ray-absorption and Mössbauer spectroscopy of $\text{EuNi}_2\text{Si}_{2-x}\text{Ge}_x$, *Phys. Rev. B* **43**, 5261 (1991).
- [31] P. Maślankiewicz and J. Szade, Valence instability of europium in EuCo_2Si_2 , *J. Alloys Compd.* **423**, 69 (2006).
- [32] I. Mayer and I. Felner, Europium silicides and germanides of the EuM_2X_2 type: Crystal structure and the valence states of europium, *J. Phys. Chem. Solids* **38**, 1031 (1977).
- [33] A. Palenzona, S. Cirafici, and P. Canepa, High temperature behaviour of the mixed valence compounds EuCu_2Si_2 , YbCu_2Si_2 and the ref-

- erence compounds CaCu_2Si_2 and GdCu_2Si_2 , *J. Less-Common Met.* **119**, 199 (1986).
- [34] I. Felner and I. Nowik, Magnetism and hyperfine interactions in $\text{Eu}M_2\text{Ge}_2$ and $\text{Gd}M_2\text{Ge}_2$ ($M = \text{Mn, Fe, Co, Ni, Cu}$), *J. Phys. Chem. Solids* **39**, 767 (1978).
- [35] I. Felner and I. Nowik, Local and itinerant magnetism and superconductivity in RRh_2Si_2 ($R = \text{rare earth}$), *Solid State Commun.* **47**, 831 (1983).
- [36] B. Kuzhel, B. Belan, V. Kuzhel, I. Stets', and R. Serkiz, Contribution of unstable valence states of europium to the electronic transport properties of $\text{EuPd}_{2-x}\text{Si}_{2+x}$, *Chem. Met. Alloys* **3**, 83 (2010).
- [37] M. Francois, G. Venturini, J. Maréché, B. Malaman, and B. Roques, De nouvelles séries de germaniures, isotopes de $\text{U}_4\text{Re}_7\text{Si}_6$, ThCr_2Si_2 et CaBe_2Ge_2 , dans les systèmes ternaires R-T-Ge où R est un élément des terres rares et $T \equiv \text{Ru, Os, Rh, Ir}$: supraconductivité de LaIr_2Ge_2 , *J. Less-Common Met.* **113**, 231 (1985).
- [38] A. Prasad, V. K. Anand, Z. Hossain, P. L. Paulose, and C. Geibel, Anisotropic magnetic behavior in EuIr_2Ge_2 single crystal, *J. Phys.: Condens. Matter* **20**, 285217 (2008).
- [39] I. Felner and I. Nowik, Local and itinerant Magnetism AND Crystal structure of RRh_2Ge_2 and RRu_2Ge_2 ($r = \text{rare earth}$), *J. Phys. Chem. Solids* **46**, 681 (1985).
- [40] S. Banik, A. Bendouan, A. Thamizhavel, A. Arya, P. Risterucci, F. Sirotti, A. K. Sinha, S. K. Dhar, and S. K. Deb, Electronic structure of EuCu_2Ge_2 studied by resonant photoemission and x-ray absorption spectroscopy, *Phys. Rev. B* **86**, 085134 (2012).
- [41] W. Iha, T. Yara, Y. Ashitomi, M. Kakihana, T. Takeuchi, F. Honda, A. Nakamura, D. Aoki, J. Gouchi, Y. Uwatoko, T. Kida, T. Tahara, M. Hagiwara, Y. Haga, M. Hedo, T. Nakama, and Y. Ōnuki, Electronic States in $\text{EuCu}_2(\text{Ge}_{1-x}\text{Si}_x)_2$ Based on the Doniach Phase Diagram, *J. Phys. Soc. Jpn.* **87**, 064706 (2018).
- [42] R. E. Gladyshevskii and E. Parthe, Crystal structure of europium dirhodium digermanium, EuRh_2Ge_2 with ThCr_2Si_2 type, *Z. Kristallogr.* **198**, 173 (1992).
- [43] I. Mayer, J. Cohen, and I. Felner, The crystal structure of the MAu_2Si_2 rare earth compounds, *J. Less-Common Met.* **30**, 181 (1973).
- [44] M. Abd-Elmeguid, C. Sauer, U. Köbler, W. Zinn, J. Röhler, and K. Keulerz, Valence instability in magnetically ordered $\text{Eu}(\text{Pd}_{1-x}\text{Au}_x)_2\text{Si}_2$, *J. Magn. Magn. Mater* **47-48**, 417 (1985).
- [45] F. Honda, K. Okauchi, A. Nakamura, D. Aoki, H. Akamine, Y. Ashitomi, M. Hedo, T. Nakama, and Y. Ōnuki, Pressure Evolution of Characteristic Electronic States in EuRh_2Si_2 and EuNi_2Ge_2 , *J. Phys.: Conf. Ser.* **807**, 022004 (2017).
- [46] S. Schulz, I. A. Nechaev, M. Güttler, G. Poelchen, A. Generalov, S. Danzenbächer, A. Chikina, S. Seiro, K. Kliemt, A. Y. Vyazovskaya, T. K. Kim, P. Dudin, E. V. Chulkov, C. Laubschat, E. E. Krasovskii, C. Geibel, C. Krellner, K. Kummer, and D. V. Vyalikh, Emerging 2D-ferromagnetism and strong spin-orbit coupling at the surface of valence-fluctuating EuIr_2Si_2 , *npj Quantum Mater.* **4**, 26 (2019).
- [47] D. Y. Usachov, A. V. Tarasov, S. Schulz, K. A. Bokai, I. I. Tupitsyn, G. Poelchen, S. Seiro, N. Carocanals, K. Kliemt, M. Mende, K. Kummer, C. Krellner, M. Muntwiler, H. Li, C. Laubschat, C. Geibel, E. V. Chulkov, S. I. Fujimori, and D. V. Vyalikh, Photoelectron diffraction for probing valency and magnetism of 4f-based materials: A view on valence-fluctuating EuIr_2Si_2 , *Phys. Rev. B* **102**, 205102 (2020).
- [48] P. G. Pagliuso, J. L. Sarrao, J. D. Thompson, M. F. Hundley, M. S. Sercheli, R. R. Urbano, C. Rettori, Z. Fisk, and S. B. Oseroff, Antiferromagnetic ordering of divalent Eu in EuCu_2Si_2 single crystals, *Phys. Rev. B* **63**, 092406 (2001).
- [49] I. Kawasaki, S.-i. Fujimori, Y. Takeda, H. Yamagami, W. Iha, M. Hedo, T. Nakama, and Y. Ōnuki, Electronic states of EuCu_2Ge_2 and EuCu_2Si_2 studied by soft x-ray photoemission spectroscopy, *Phys. Rev. B* **100**, 035111 (2019).
- [50] G. K. Woodgate, *Elementary atomic structure*, European physics series (McGraw-Hill, London, New York, 1970).
- [51] T. Hotta, Effect of Spin-Orbit Coupling on Kondo Phenomena in f^7 -Electron Systems, *J. Phys. Soc. Jpn.* **84**, 114707 (2015).